Dual-Axis Torsional Thrust Stand for Simultaneous Direct Measurement of Thrust and Mass Loss

IEPC-2019-A139

Presented at the 36th International Electric Propulsion Conference
University of Vienna, Austria
September 15-20, 2019

Matthew R. Gilpin,* Michael R. Natisin,†
Carlos Marin,‡ Michael D. Eschen,§ and Henry L. Zamora¶
ERC Incorporated, Edwards AFB, CA 93524

A dual-axis torsional thrust stand has been constructed at the AFRL to enable direct simultaneous thrust and mass loss measurements for electrospray thrusters. The dual-axis system is effectively two conventional, nulled, torsional thrust stands nested within one another with a measurement range of ± 1200 μN and ± 70 mg. Proof of concept data taken using the in-house AFET-2 electrospray thruster has successfully demonstrated simultaneous measurements in the short term (hours). Long-term (days) thrust stand operation is currently limited by cyclic drift induced by ambient temperature changes and the resulting orientation shift in the thrust stand platform. A novel approach was taken to control the effects of platform shift by applying known perturbations and using the resulting thrust stand response to calculate the location of the center of gravity (CG) in-situ. The CG can then be centered to reduce drift sensitivity. This method has successfully characterized and controlled drift for the "mass axis" keeping observed cyclic drift within ± 0.5 mg. The "thrust axis", however, is not fully characterized by CG placement and a yet uncharacterized drift contribution yields cyclic drift of $\pm$ 8 μN which is an order of magnitude above the design goal.

Nomenclature

CG	= center of gravity location
(cg_x, cg_y, cg_z)	= CG coordinates in the thrust stand coordinate system
$\vec{g}$	= gravity vector
$(g'_{\theta x}, g'_{\theta y}, g'_{\theta z})$	= gravity vector components in $\{x, y, z\}$ after rotation in θ
$(g'_{\phi x}, g'_{\phi y}, g'_{\phi z})$	= gravity vector components in $\{x, y, z\}$ after rotation in ϕ
$(g'_{\theta x-\beta}, g'_{\theta y-\beta}, g'_{\theta z-\beta})$	= gravity vector components in $\{x, y, z\}$ after rotation in θ and β
$(g'_{\phi x-\beta}, g'_{\phi y-\beta}, g'_{\phi z-\beta})$	= gravity vector components in $\{x, y, z\}$ after rotation in ϕ and β
h	= z coordinate of $\vec{g}$ in $\{x, y, z\}$ after rotation in both θ and ϕ
$\{x, y, z\}$	= thrust stand coordinate system
$\{x_{table}, y_{table}, z_{table}\}$	= tilt platform coordinate system
$\{x'_\theta, y'_\theta, z'_\theta\}$	= Earth coordinate system after rotation in θ
$\{x'_\phi, y'_\phi, z'_\phi\}$	= Earth coordinate system after rotation in ϕ

*Spacecraft Propulsion Consultant, In-Space Propulsion Branch AFRL/RQRS, matthew.r.gilpin.ctr@us.af.mil
†Research Scientist, In-Space Propulsion Branch AFRL/RQRS, michael.natisin.ctr@us.af.mil
‡Propulsion Engineer, In-Space Propulsion Branch AFRL/RQRS, cmarin@usc.edu
§Propulsion Engineer, In-Space Propulsion Branch AFRL/RQRS, eschen@usc.edu
¶Propulsion Engineer, In-Space Propulsion Branch AFRL/RQRS, henry.zarmora.ctr@us.af.mil

β = alignment angle between $\{x, y, z\}$ and $\{x_{table}, y_{table}, z_{table}\}$ about z
θ = tilt angle about y
ϕ = tilt angle about x
τ_m = torque about the mass axis, x
τ_t = torque about the thrust axis, z

I. Introduction

A new dual-axis torsional thrust stand capable of simultaneous thrust and mass loss measurement is being investigated at the United States Air Force Research Laboratory (AFRL) in support of in-house electrospray thruster development.[1] The use of torsional thrust stands for electrospray measurements is well documented[2–4] and in-situ measurement of thrust and mass loss using analytical balances has also become common practice.[5–7] However, the use of separate diagnostics or separate tests for time resolved thrust and mass loss measurement requires the combination of two data sets and assumes that both tests were conducted under identical conditions. What is unique about the diagnostic presented here is the continuous, simultaneous measurement of both quantities allowing direct comparison between thrust and mass loss for the same test.

Having simultaneous thrust and mass loss measurements is of particular importance to the development of porous-media-based electrospray thusters at the AFRL. In these designs, the entire propellant supply and feed system is fully housed within the thruster itself, rather than provided via an external fuel tank or feed line, removing the ability to perform direct in-situ measurement of the mass flow rate since the flow cannot be externally measured or controlled. Additionally, the emitters and propellant of these thrusters are exposed to the local atmosphere and care must be taken to limit exposure to non-vacuum conditions so that performance isn't effected. The current method of measuring mass change before and after testing requires that quantities of interest such as propulsion efficiency and specific impulse be averaged throughout a test and also exposes the thruster to atmosphere during the measurement process. A simultaneous measurement capability will allow for performance data to be directly calculated under known conditions, without averaging and without breaking vacuum.

II. Design Concept

The dual-axis thrust stand is effectively two conventional nulled torsional thrust stands nested within one another enabling simultaneous measurement of torques about a "thrust axis" and a "mass axis." Management of long term drift for both axes is the limiting factor to successful measurements and the design presented here was primarily concerned with with the characterization and minimization of drift associated with changes in the thrust stand platform orientation as a function of time. Instead of the typical practice of maintaining platform orientation to be orthogonal with gravity, an alternative approach was taken to reduce the overall sensitivity to gravity vector orientation by measuring and centering the thrust stand center of gravity (CG). The thrust stand is mounted on a platform which is able to assign known tilts to the thrust stand and the response of these tilts is used to calculate the location of the GC. By providing an in-situ CG measurement capability, the CG can be centered to reduce overall tilt sensitivity below the desired system resolution.

A. General Arrangement

The general arrangement and coordinate system for the dual-axis thrust stand is given in Fig. 1. At the center of the stand is a two axis gimbal supported by flexural pivots, with the outer assembly allowing rotation about the vertical "thrust axis" (z) and the inner assembly allowing rotation about the horizontal "mass axis" (x). The thrust stand beam, located at the center of the gimbal, has two degrees of freedom and the thruster is mounted on the left hand side of the beam.

Two plates running parallel to the thrust stand beam are attached to the inner gimbal assembly which restricts their rotation to only about the thrust axis. Calibration and control equipment for the mass axis are attached to these plates and ride along with the thrust axis during operation. This configuration is required to eliminate the effects of off axis forces from the calibration and control hardware and ensure that forces are only applied to the desired axis.

The flexural pivots supporting the dual-axis gimbal have an approximate spring constant of 0.076 Nm/rad

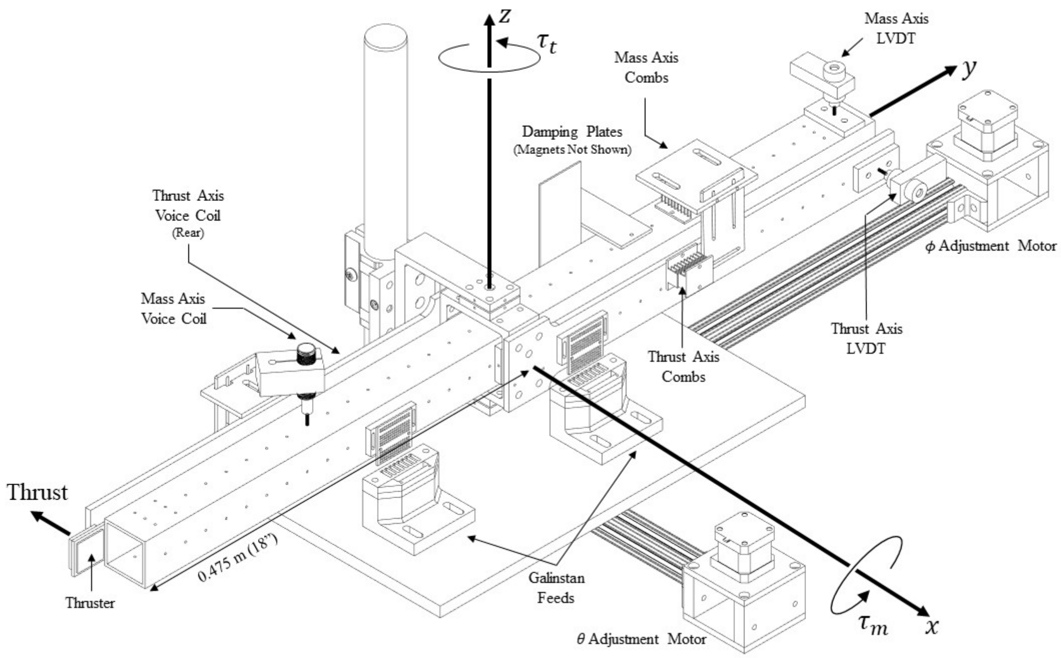

Figure 1. Drawing of the dual-axis thrust stand defining the coordinate system, each axis of rotation and positive torque directions.

in each rotation direction. This effectively limits the fundamental sensitivity of the system to 0.1 μNm on either axis as a finite torque is required to cause sufficient signal for the control system. Despite this resolution limitation, it is practically beneficial to have a finite spring constant on each axis as this allows the thrust stand to "float" when not under active control simplifying the alignment process prior to operation.

Both axes utilize identical calibration and control arrangements. Rotation is recorded at 100 ms intervals using two linearly variable differential transformers (LVDT) assuming small deflections and two LabView based PID controllers are used to supply current to the voice coils. Coil currents are recorded by measuring voltage drop across 10 Ω shunt resistors which are capable of sustaining $< 1\%$ change in resistance up to a maximum of 10 W per channel. Electrostatic combs[4,8,9] are used to provide known torques to each axis in order to calibrate the voice coils after the nulling system has been activated. Damping is provided by both passive eddy current damping, allowing the system to come to an equilibrium when not under control, and through the voice coils so that behavior can be adjusted.

The stand was designed using a nulled configuration primarily to eliminate consideration of coupled rotational dynamics and to maintain a fixed neutral position. The PID system is capable of holding each axis to $\pm$ 1.5 μRad and thus it is assumed that both axes are fixed and orthogonal during operation. A nulled configuration also is the standard design for analytical balances and high sensitivity comparator balances[10,11] which inspired design of the mass axis.

A stepper driven traverse is embedded within the thrust stand beam running parallel to the y axis. This traverse is capable of moving a 100 g mass in 5 μm increments and is used to balance the mass axis of the stand prior to operation. Initial balance of the mass axis is critical as any torque required to "zero" the system takes away from the maximum measurement range and initial balance capability should be on the order of the desired measurement resolution. For a nominal measurement resolution of 0.5 mg, manual balancing would require the use of either $< mg$ weights at the location of the thruster, or $< mm$ placement precision of a 1 g mass making manual balancing impractical. A physical balance mechanism (as opposed to a second voice coil dedicated to zeroing) is required by the tilt sensitivity concerns discussed in Section I.B and can also be used to de-saturate the mass axis during extended testing.

Two sets of galinstan pools are used to feed power to the thruster, mass axis calibration and control hardware, and the y axis traverse. The first set of galinstan pools are used to provide power to the mass axis hardware and are mounted to the thrust axis plates (one degree of freedom). The second set of pools are mounted to the thrust stand beam (two degrees of freedom) and are used to feed power to the thruster and the y axis traverse. The successful use of liquid metal pools for thrust stand connections is documented in the literature.[4,12] However, in this application what are presumed to be electrostaic effects within the galinstan feeds are observed whos magnitude follows V^2 scaling. For example, when 2000 V are applied to a thruster without propellant, the system registers ≈ 3.5 μN of steady state thrust and 1 mg of mass loss. These spurious forces negatively effect current performance, but careful re-engineering of the galinstan feeds incorporating sufficient shielding should alleviate these issues in future designs.

As presented here, the dual-axis thrust stand system has a maximum range of ± 1200 μN and ± 70 mg for a thruster mounted 0.511 m (20.125") from the center. All results are presented as thrust stand output for a thruster at this location.

B. Tilt Sensitivity

The primary concern during the development of the dual-axis thrust stand was characterization and reduction of torques due to orientation changes of the thrust stand platform. Heating, ventilation and air conditioning (HVAC) induced thermal cycling of the testing chamber produces observed tilts of approximately ± 1 $mrad$ and the resulting shifts in the relative direction of the gravity vector can saturate thrust stand measurements if the system is improperly designed.

Changes to the relative direction of the gravity vector will impart torques on both axis of the stand if the overall CG is not centered at the intersection of the thrust and mass axis. The dependence of drift and overall noise sensitivity on CG location is a known concern and was well documented for a horizontal dynamic torsional pendulum by Ziemer.[2] With the understanding that having a perfectly balanced thrust stand and perfectly horizontal rotational plane is difficult in practice, Ziemer's design mounted the thrust stand on a leveling platform and active control was used to keep the thrust stand axis of rotation parallel with the gravity vector. This active control scheme is standard practice for torsional balances which achieve long term stability,[2,3,13] as is using counterweights to center the CG.[4]

For the dual-axis thrust stand a different design approach was considered. Instead of using a leveling platform to actively correct for changes in orientation, the leveling platform was used here to provide known tilts to the thrust stand in order to determine the location of the thrust stand CG in-situ. If the CG can be located and centered with sufficient precision, the sensitivity of the thrust stand to platform orientation can be reduced below the desired resolution with the added benefit of reducing sensitivity to vibration.[2] For this work, the CG location was adjusted manually but ultimate design goal for this system is to have remotely adjustable masses along all three principle axes allowing for CG manipulation after thruster install without breaking vacuum.

The tilt angles θ and ϕ for the thrust stand are defined as shown in Fig. 2. Since the thrust stand is operated in a nulled configuration, the orientation of the stand with respect to the tilt platform is assumed to be constant. In this analysis the coordinate system attached to the thrust stand, $\{x, y, z\}$, is assumed to be fixed and changes in platform orientation alter the relative orientation of the gravity vector. Furthermore, it is assumed that all axis are orthogonal and that the tilt platform is properly aligned with the thrust stand. The effects of this final assumption are discussed in detail in Appendix A and the relative insensitivity of the system to misalignment means that this assumption can be met without extensive engineering effort.

Figure 3 shows the effects of orientation change on the gravity vector and how this relates to each axis of the thrust stand when θ and ϕ are applied separately. For the thrust axis, tilt about θ produces a component of the gravity vector that is parallel to the x axis and tilt about ϕ produces a component of the gravity vector parallel to the y axis. For the given CG location, the induced torque about the thrust axis is

$$\tau_t \approx |\vec{g}| sin(\phi) cg_x m - |\vec{g}| sin(\theta) cg_y m \tag{1}$$

noting that cg_z location does not have an effect on torque about the z axis and if the small angle approximation is used, then the torques induced by ϕ and θ will vary linearly with angle. The relationship in Eq. 1 is approximate because with simultaneous tilt in ϕ and θ, the gravity components $g'_{\theta x}$ and $g'_{\phi y}$ are coupled. However, as discussed in Appendix A, this coupling effect is negligible.

If the thrust stand platform is used to apply known values of ϕ and θ to the thrust stand, the resuling torques can be recorded and the following relations can be used to determine the location of cg_x and cg_y for the thrust axis.

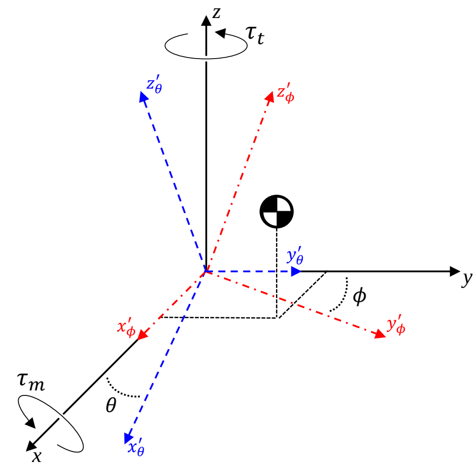

Figure 2. Definition of orientation angles θ, for rotation about the y, and ϕ for rotation about x. The primed coordinates represent the coordinate system of the earth with respect to the fixed $\{x, y, z\}$ corrdinate system assigned to the thrust stand.

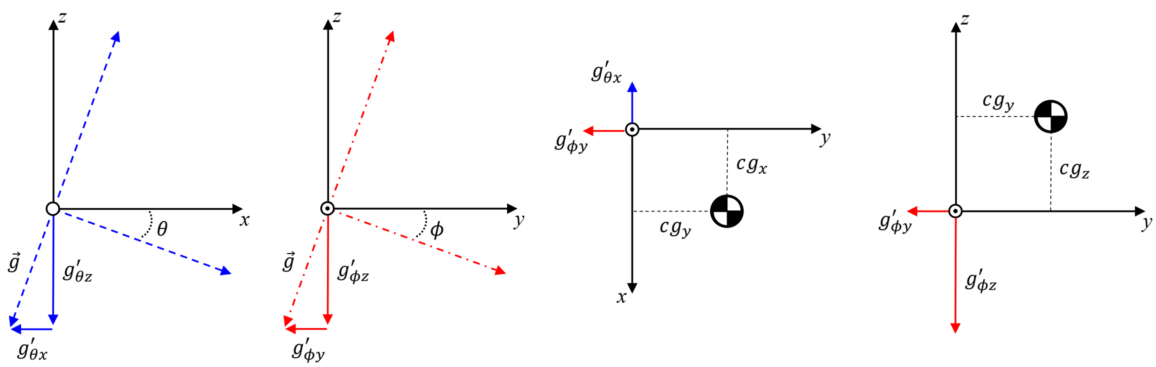

Figure 3. From left to right: Gravity vector components with respect to the thrust stand after tilt in θ, gravity vector components after tilt in ϕ, gravity vector components and CG location orthogonal to the thrust axis, gravity vector components and CG location orthogonal to the mass axis.

$$\frac{\partial \tau_t}{\partial \phi} \approx -|\vec{g}|cg_x m \qquad \frac{\partial \tau_t}{\partial \theta} \approx |\vec{g}|cg_y m \tag{2}$$

Tilt sensitivity for the mass axis is dependent on ϕ since changes in θ produce a gravity component parallel to the axis of rotation. As there are two torque components that change with a change in ϕ, experimental determination of the mass axis CG location requires the assumption that $cg_y = 0$ for the mass axis hardware (i.e. cg_y of only the hardware with two degrees of freedom) which is reasonable because prior to operation, the thrust stand is balanced using the internal stepper motor assembly discussed in Section I.A. For any cg_y component remaining, it can also be noted that changes in $g'_{\phi z}$ are proportional to $cos(\phi)$ who's derivative is minimal under the small angles considered here further aiding this assumption.

Assuming cg_y is negligible for the mass axis hardware, the induced torque about the mass axis can then be calculated as

$$\tau_m \approx |\vec{g}|sin(\phi)cg_z m \tag{3}$$

and application of the small angle approximation allows for cg_z to be calculated from experimentally measured sensitivity with respect to ϕ.

$$\frac{\partial \tau_m}{\partial \phi} \approx |\vec{g}| cg_z m \tag{4}$$

Equations 2 and 4 allow the CG location to be determined experimentally and then re-centered.

Considering an HVAC induced tilt of ± 1 $mrad$ in both ϕ and θ, a sensitivity of ± 1 μN for a thruster mounted 0.511 m (20.125") requires that both $\partial \tau_t / \partial \phi$, $\partial \tau_t / \partial \phi \approx 0.25$ $\mu Nm/mrad$. Assuming an equivalent mass of 100 g, this would require cg_x and cg_y placement accuracy of ≈ 0.25 mm. For a mass axis sensitivity of ± 0.1 mg, $\partial \tau_m / \partial \phi \approx 0.5$ $\mu Nm/mrad$ requiring that cg_y be placed within ≈ 0.5 mm with an equivalent balance mass of 100 g. CG locations are presented in the remainder of this paper as the location of a 100 g mass yielding an equivalent torque to what is observed from the thrust stand.

C. Thermal Sensitivities

The design of the current thrust stand did not strive to optimize thermal sensitivities, but characterization was performed at atmosphere in an insulated isolation box to reduce effects from thermal gradients. Thermal sensitivity of the mass axis is well understood due to the care taken in the comparator balance literature. For a mass balance, length stability is critical and must remain stable within the same fractional amount as the desired mass resolution.[10,14] The mass axis assembly for the current thrust stand is approximately 1.5 kg so differential thermal expansion of the thrust stand beam results in the shift of 0.75 kg equivalent masses. For a measurement resolution of $\pm$ 0.5 mg, and assuming that mass is evenly distributed throughout the system, this requires that differential temperatures be maintained within $\approx$0.06 $^{\circ}C$.

For the thrust axis, strong thermal dependence has been observed which is not well characterized and appears to be the dominant force in the overall drift. Future work on the dual-axis system will be focused on characterizing this thermal effect.

III. Operation Procedure

The operation of the dual-axis thrust stand begins by performing an initial alignment without activating the nulling system to ensure that the neutral position of both LVDTs is about zero, maximizing the potential measurement range. After this initial alignment, the nulling system is activiated and electrostatic combs are used to provide known torques and calibrate the response of both voice coils. Known tilts are then applied to the stand to record tilt sensitivities completing in-situ system characterization.

A. Voice Coil Calibration

Calibration of the voice coils is performed each time the nulling system is activated and is repeated throughout testing to confirm proper stand operation. Voltages between 150 - 600 V are applied to two sets of electrostatic combs to provide known steady state forces to each axis and the resulting nulling current is then recorded. Sample calibration results for each axis are given in Figure 4. It has been observed that coil calibrations vary <1% during multiple days of operation.

B. Center of Gravity Manipulation

The thrust stand platform is used to apply known tilts in θ and ϕ to the stand while recording the changes in nulling torque applied. Example data for part of this process is given in Fig. 5 demonstrating the response from each axis to changes in ϕ. So long as absolute angles remain within the small angle approximation, CG characterization data is related to relative changes as opposed to absolute values with any initial misalignment reflected in the "zero" signal from the voice coils.

The recorded sensitivity for each axis is used to calculate the location of the CG via Eqs. 2 and 4 and the results of three rounds of CG adjustment are given in Fig. 6 demonstrating the ability to reduce overall sensitivity. The improvements shown in Fig. 6 are relatively course due to the current manual CG adjustment scheme which relies on the available thrust stand hole spacing. This process also requires a full system reset

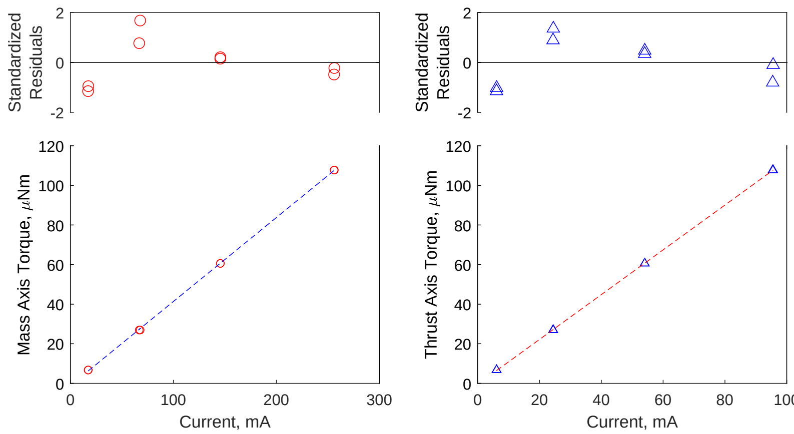

Figure 4. Example voice coil calibration data for the thrust axis and mass axis. Known torques are applied using electrostatic combs and the nulling current supplied to each voice coil is measured across a shunt resistor.

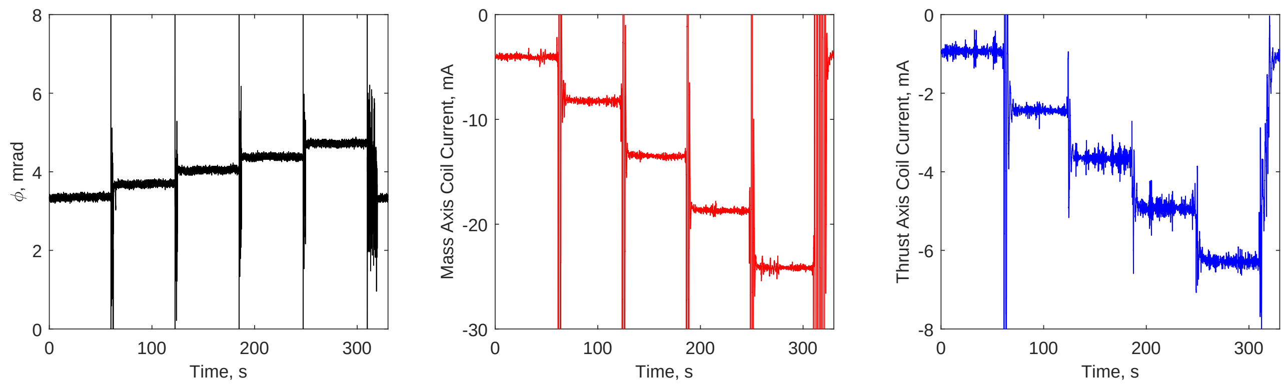

Figure 5. Example thrust stand response to known tilt application in ϕ. The sharp noise in the inclinometer data is induced by the tilt platform motors and the corresponding noise in each axis are oscillations as the control system reacts to the platform disturbance. Data is captured in the steady state regions after the system has settled.

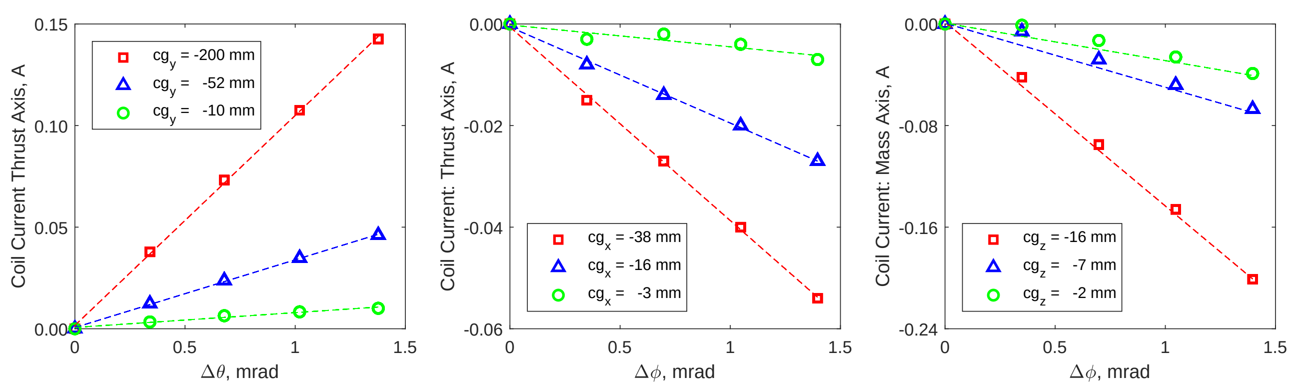

Figure 6. Tilt sensitivity results for three iterations of CG adjustment showing the overall reduction of sensitivity to platform tilt. Values for CG locations assume a 100 g equivilant mass.

after each manual adjustment. Future work will incorporate a remote system enabaling fine adjustment along each dimension so sensitivity reduction can be performed in-situ in quick succession.

IV. Current Results

The dual-axis thrust stand was installed in the "Chamber 2" electrospray test facilty at the In-Space Propulsion Branch of the AFRL at Edwards AFB and tests were conducted using the AFET-2 thruster. This test campaign successfully produced short duration proof-of-concept data demonstrating simultaneous thrust and mass loss measurements for an electrospray. Drift characterization was also successful in quantifying long term drift for the mass axis. Thrust axis drift was not succesfully characterized by measured tilt sensitivities and is an order of magnitude above the desired resolution.

A. Proof of Concept Data

Figure 7 shows simultaneous thrust and mass loss values recorded for a 2.4 hour firing of the AFET-2 thruster at a constant emitter voltage of 1700 V. Both thrust and mass data has been corrected by removal of approximated linear drift and spurious electrostatic effects in the galinstan feeds are expected to be 0.75 mg on the mass axis and 3.5 μN on the thrust axis.

Total mass loss data agrees within $\pm$ 2.5% to analytical balance measurements before thruster installation and immediately after removal from the testing chamber. It must be noted that during the available testing window only one successful complete data set was captured. However, the reported mass loss uncertainty is similar to that observed in atmosphere for pipet delivered water droplet evaporation tests.

Unexpectedly, oscillations are present on both axes when the thruster is operating and were observed to correspond with a charge-discharge cycle of dielectric surfaces within sight of the thruster plume. Fig. 8 shows that the effects of this process are synchronous on both axes and it was visually observed that oscillations were preceded by a discharge from an undetermined source to the grounded table below the thrust stand platform. The thrust stand platform was constructed using an anodized aluminum plate with anodized framing. This will be replaced in the future with non-anodized versions to reduce potential locations for charge accumulation.

Proof of concept data shows that the dual-axis thrust stand is capable of simultaneous measurements in the short term. However, significant engineering work remains to create a reliable diagnostic for extended multi-day tests.

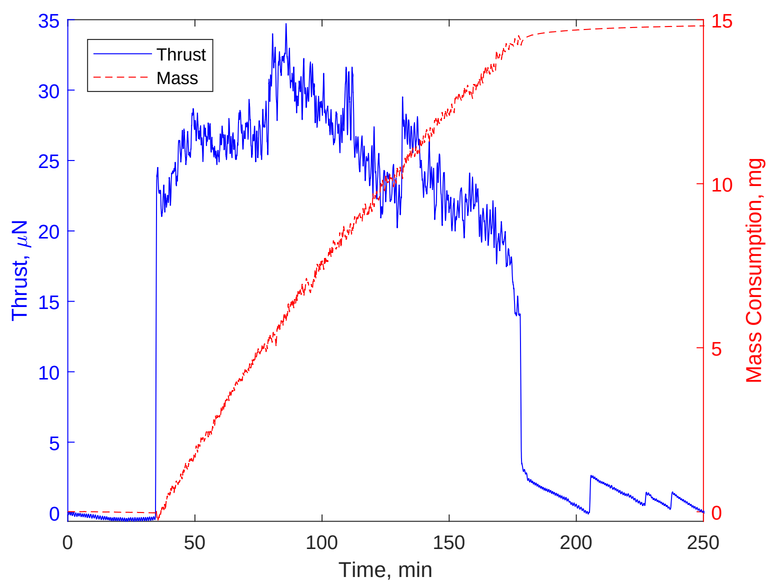

Figure 7. Simultaneous thrust and mass loss data for a 2.4 hour firing of the AFET-2 thruster using EMI-BF4 propellant and a constant emitter voltage of 1700 V. Data has been filtered using a 25 second moving average and linear drift has been removed. Mass loss values agree with pre-post measurements on an analytical balance within $\pm$2.5%

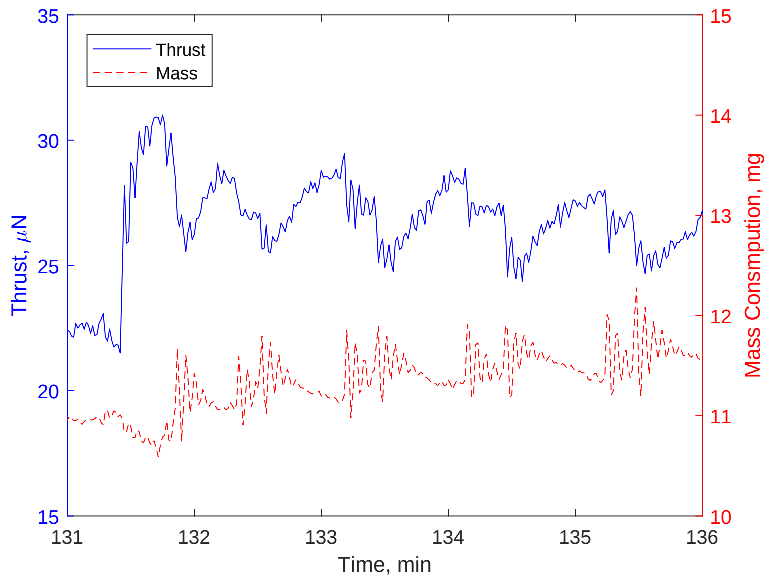

Figure 8. Zoomed, un-filtered view of the proof of concept data in Fig. 7 to highlight the disturbances in both the thrust and mass axis which were synced with an observed visible electric discharge to the grounded chamber platform. For the mass axis data, oscillations are occurring at the natural frequency and the response is indicative of a long build up (charge) and sudden release of force (discharge) which leads to second order behavior.

B. Drift Characterization

The thrust stand is currently capable of taking short term measurements by linearly approximating drift and removing it from the signal in keeping with standard practice. However, a reliable diagnostic for muli-day operation requires that long term drift be below the desired measurement resolution.

Example drift characterization data is given in Fig. 9 highlighting the dependence of platform motion and thrust stand drift on the ambient temperature with all measured quantities showing synced cyclic transients. In the case of platform orientation, there is also a net trend dependent on the moving average of the ambient temperature.

The mass axis was well characterized by the measured tilt sensitivity and overall drift was kept within $\pm$ 0.5 mg with $cg_z = 2$ mm for a 100 g equivalent mass. To calculate the expected tilt contribution, the sensitivities $\partial\tau_m/\partial\phi$ and $\partial\tau_m/\partial\theta$ were multiplied by the measured platform angle and summed. Contrary to the assumption in Section I.B that tilt sensitivity in the mass axis is only a function of cg_z and ϕ, a linear $\partial\tau_m/\partial\theta$ is also observed when applying known tilts to the stand which contributes approximately 15 % of the expected signal and thus is not negligible. This extra contribution isn't believed to be a symptom of system misalignment, which is discussed in Appendix B, and the expected residual cg_y from the balancing procedure is nearly two orders of magnitude below whats necessary to cause this effect. Furthermore, the unknown location of cg_x for the mass axis is not expected to contribute to tilt sensitivity as it is along the axis of rotation and it's orientation remains fixed with respect to the x axis of the thrust stand regardless of platform tilt. Contribution to the mass axis from θ is as yet uncharacterized, but is not a limiting factor for long term stability at the current resolution.

For the thrust axis, platform tilt does not adequately characterize the observed drift. Similar to the mass axis, the expected thrust axis drift in Figure 9 is calculated by multiplying measured platform angles by the recorded values for $\partial\tau_t/\partial\theta$ and $\partial\tau_t/\partial\phi$. Since these quantities are directly measured, it is assumed that the expected thrust axis torque in Figure 9 is well determined. The unknown position of cg_z for the combined thrust and mass axis hardware is also assumed to have no effect as it is along the axis of rotation and remains fixed with respect to the z axis of the stand regardless of platform tilt. The tilt contribution to overall thrust stand drift is currently below an as yet uncharacterized contribution which appears to follow the cyclic behavior of the ambient temperature. This unknown contribution is an order of magnitude above

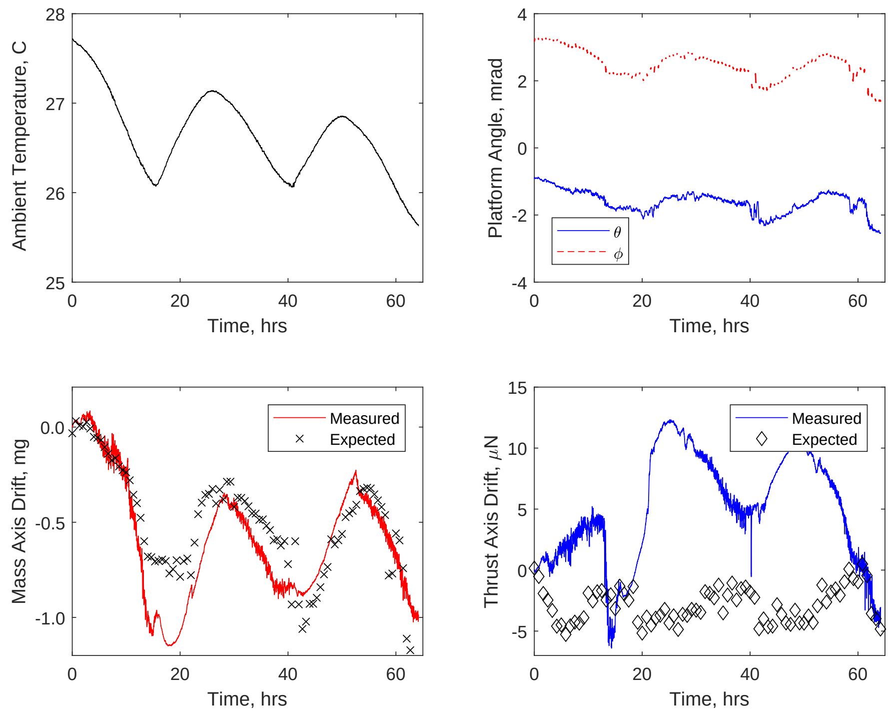

Figure 9. Example drift characterization for the dual-axis thrust stand when testing at atmosphere. Thrust stand drift is presented as the equivalent signal as opposed to absolute torque and expected torque is calculated based on inclinometer measurements and measured tilt sensitivities. Note that if absolute torque is considered, each axis demonstrates cyclic drift at the same order of magnitude.

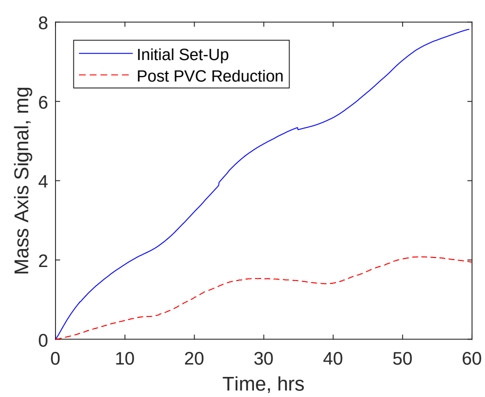

Figure 10. Quasi steady drifts observed on the mass axis beginning approximately 12 hours after pump down which demonstrate a reduction in macro drift by the removal of outgassing materials. The oscillations in each signal are comparable to drift expectations based on platform tilt if the linear macro drift slope is removed. Testing was performed at a pressure of ≈ 1 $\mu Torr$.

the desired drift resolution and is currently the limiting factor for long term testing.

Macro drift in the mass axis was also observed when testing in vacuum. For approximately 12 hours after pump down, the mass axis exhibits drift with a decaying slope followed by a transition to a quasi-linear drift. The initial reaction of the mass axis to pump down is thought to be caused by both the altered thermal environment and outgassing. The following quasi-linear region is then thought to be caused by vacuum incompatible materials with a substantial outgassing rate. The traverse contained within the thrust stand beam uses an off the shelf stepper motor which connects to the galinstan power feed with PVC insulated leads - a known vacuum-incompatible material.[15] Figure 10 shows that by shortening these PVC leads and removing approximately 10 g of PVC from the left hand side of the mass axis, the macro drift slope of the linear region is reduced by 75%. The sensitivity of the mass axis requires that care must be taken in future designs to only incorporate vacuum compatible materials and hardware.

V. Conclusion

A new dual-axis thrust stand has been designed with the goal of enabling simultaneous thrust and mass loss measurements for electrospray thrusters. The current system has successfully produced proof of concept data showing that such measurements are possible. However, further engineering work is required before the dual-axis stand becomes a reliable diagnostic for long duration testing.

The limiting factor in thrust stand performance is cyclic drift which is driven by tempertaure effects as well as changes to the thrust stand orientation with respect to gravity. The novel approach taken here, focusing on in-situ CG characterization to reduce tilt sensitivity, has successfully characterized and controlled drift for the mass axis. The primary source of thrust axis drift remains uncharacterized and will be the focus of future design iterations. Future work will also incorporate practical lessons learned during this effort including a re-design of the galinstan feed system and optimizing the thrust stand beam for the minimization of thermal gradients.

It should also be noted that, in principle, the dual-axis thrust stand is capable of providing simultaneous thrust and mass loss data for other self-contained propulsion systems by simply altering the range of the voice coils. The challenge in this work was creating a reliable system at the μN level where thrust stand drift and measurement quantities are of the same order of magnitude. Since drift sources do not directly scale with thrust level, increasing the thrust measurement range by an order of magnitude would not require substantial changes to the thrust stand and macro drift levels would remain the same.

Appendix

A. Simultaneous Tilt in θ and ϕ

Equations 1 and 3 assume that $g'_{\theta x}$ and $g'_{\phi y}$ are independent. However, these two vector components are coupled for simultaneous tilt in θ and ϕ. Figure 11 shows the location of the gravity vector with respect to the thrust stand coordinate system where the angles θ and ϕ are defined as the angle between the projection of $|\vec{g}|$ and $g'_{\theta x}$ and $g'_{\phi y}$ respectively. This is in keeping with the definition of angles reported from the inclinometers on the thrust stand platform.

The values of $g'_{\theta x}$ and $g'_{\phi y}$ can be written as

$$g'_{\theta x} = h \cdot tan(\theta) \tag{5}$$

$$g'_{\phi y} = h \cdot tan(\phi) \tag{6}$$

and as h is the third component of $|\vec{g}|$, the following is true

$$|\vec{g}|^2 = g'^2_{\theta x} + g'^2_{\phi y} + h^2 \tag{7}$$

By using Eq. 7 to solve for h, Eqs. 5 and 6 can then be used to solve for the following

$$g'_{\theta x} = \frac{|\vec{g}|}{\sqrt{tan^2(\theta) + tan^2(\phi) + 1}} tan(\theta) \tag{8}$$

$$g'_{\phi y} = \frac{|\vec{g}|}{\sqrt{tan^2(\theta) + tan^2(\phi) + 1}} tan(\phi) \tag{9}$$

which are equivalent to Eqs. 1 and 3 if tilt in only a single axis is considered. Equations 8 and 9 are within $< 0.5\%$ of Eqs. 1 and 3 for combined tilts of up to 100 $mrad$ and thus the coupling effect is considered to be negligible.

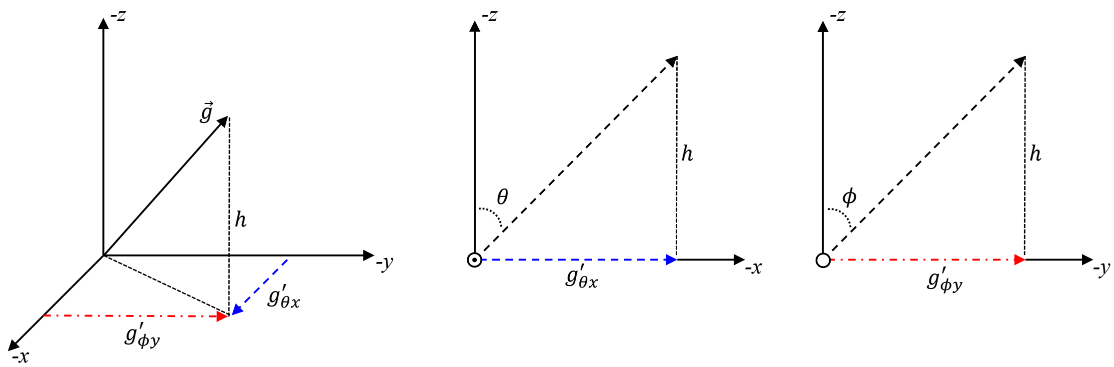

Figure 11. Gravity vector components for simultaneous tilt with θ and ϕ defined as reported by the thrust stand platform inclinometers.

B. Table Misalignment

The characterization of tilt effects in θ and ϕ are related to relative changes in orientation so misalignment between the thrust stand and the tilt table as well as initial misalignment between the thrust stand and the earth frame for these rotation angles will not affect measurements of CG location, only the initial torques applied to zero each axis. Rotational misalignment between the thrust stand and the tilt table will have an effect on measured CG values and will create a θ dependence for the mass axis not accounted for in the assumptions given in Section I.B.

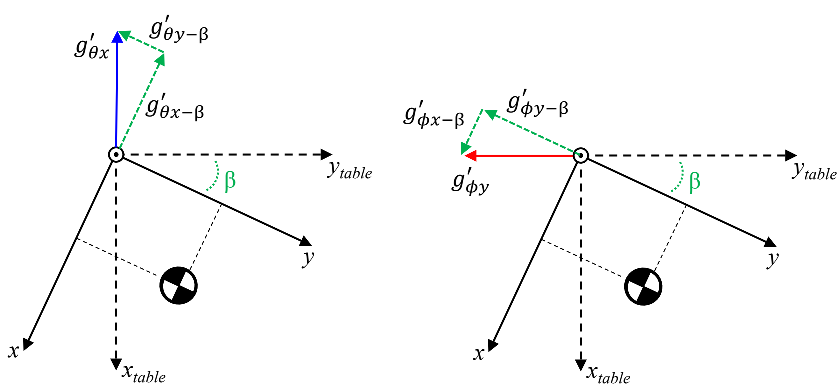

Figure 12. Gravity vector components for tilt in θ and ϕ considering a rotational misalignment about the z axis, β, between the thrust stand and the tilt table.

Figure 12 shows gravity vector components considering an initial rotational misalignment between the thrust stand and the thrust stand platform. Misalignment, defined by the angle β, effects the gravity vector components created by tilt θ and ϕ and alters Eqs. 1 and 3 so that induced torques become

$$\tau_t \approx |\vec{g}|\{sin(\phi)cos(\beta) + sin(\theta)sin(\beta)\}cg_x m - |\vec{g}|\{sin(\theta)cos(\beta) + sin(\phi)sin(\beta)\}cg_y m \quad (10)$$

$$\tau_m \approx |\vec{g}|\{sin(\theta)sin(\beta) + sin(\phi)cos(\beta)\}cg_z m \quad (11)$$

These new induced torques are within 1% of Eqs. 1 and 3 for $\beta < 0.01\ rad$ which is achievable within standard machining tolerances. Thus it is assumed that effects of β can be negligible with appropriate system design.

For the mass axis, misalignment in β will add a linear torque dependence on θ due to the $g'_{\theta y - \beta}$ gravity component. As mentioned in Section IV.B, a linear dependence with θ was observed during thrust stand characterization. However, the magnitude of the $\partial\tau_m/\partial\theta$ observed for the test in Fig. 9 would require $\beta \approx 0.2\ rad$ which is unreasonable with even a cursory alignment prior to testing.

Acknowledgments

This work was funded by the United States Air Force Research Laboratory, Aerospace Systems Directorate, In-Space Propulsion Branch.

References

[1]Natisin, M. R., Zamora, H. L., Holmes, M., and Eckhard, D., "Performance of a Fully Conventionally Machined Liquid-Ion Electrospray Thruster Operated in PIR," *36th International Electric Propulsion Conference*, Vienna, Austria, Sept. 2019.

[2]Ziemer, J. K., "Performance Measurements Using a Sub-Micronewton Resolution Thrust Stand," *27th International Electric Propulsion Conference*, No. IEPC-01-238, Pasadena, CA, Oct. 2001.

[3]Gamero-Castaño, M., "A Torsional Balance for the Characterization of MicroNewton Thrusters," *Review of Scientific Instruments*, Vol. 74, No. 10, July 2003, pp. 4509–4514.

[4]Polk, J. E., Pancotti, A., Haag, T., King, S., Walker, M., Blakely, J., and Ziemer, J., "Recommended Practice for Thrust Measurement in Electric Propulsion Testing," *Journal of Propulsion and Power*, Vol. 33, No. 3, May 2017, pp. 539–555.

[5]Courtney, D., Dandavino, S., and Shea, H., "Comparing Direct and Indirect Thrust Measurements from Passively Fed and Highly Ionic Electrospray Thrusters," *Journal of Propulsion and Power*, Vol. 32, No. 2, March 2016.

[6]Courtney, D. G. and Shea, H., "Charge Neutralization and Direct Thrust Measurements from Bipolar Pairs of Ionic-Electrospray Thrusters," *Journal of Spacecraft and Rockets*, Vol. 55, No. 1, Jan. 2017.

[7]Courtney, D. G., Alvarez, N., and Demmons, N. R., "Electrospray Thrusters for Small Spacecraft Control: Pulsed and Steady State Operation," *AIAA/ASME/SAE/ASEE Joint Propulsion Conference*, Cincinnati, Ohio, July 2018.

[8]Selden, N. P. and Ketsdever, A. D., "Comparison of Force Balance Calibration Techniques for the Nano-Newton Range," *Review of Scientific Instruments*, Vol. 75, No. 12, Sept. 2003.

[9]Pancotti, A. P., Gilpin, M., and Hilario, M. S., "Comparison of Electrostatic Fins with Piezoelectric Impact Hammer Techniques to Extend Impulse Calibration Range of a Torsional Thrust Stand," *Review of Scientific Instruments*, Vol. 83, No. 3, Feb. 2012.

[10]Quinn, T. J., Speake, C. C., and Davis, R. S., "A 1 kg Mass Comparator Using Flexure-Strip Suspensions: Preliminary Results," *Metrologia*, Vol. 23, No. 2, Jan. 1986, pp. 87–100.

[11]Quinn, T. J., "The Beam Balance as an Instrument for Very Precise Weighing," *Measurement Science and Technology*, Vol. 3, No. 2, Feb. 1992, pp. 141–159.

[12]Polzin, K. A., Markusic, T. E., Stanojev, B. J., DeHoyos, A., and Spaun, B., "Thrust stand for electric propulsion performance evaluation," *Review of Scientific Instruments*, Vol. 77, No. 10, Oct. 2006, pp. 105108.

[13]Haag, T. W., "Thrust Stand for Pulsed Plasma Thrusters," *Review of Scientific Instruments*, Vol. 68, No. 5, May 1997, pp. 2060–2067.

[14]Schoonover, R. M. and Taylor, J. E., "Some Recent Developments at NBS in Mass Measurements," *IEEE Transactions on Instrumentation and Measurement*, Vol. IM-35, No. 4, Dec. 1986, pp. 418–422.

[15]Thomas, D., editor, *Spacecraft Material Outgassing Data*, No. NASA-0000111, National Aeronautics and Space Administration, 2018.